JOURNAL OF MATERIALS SCIENCE **39** (2004) 7183–7191

Transient VAR ingot growth modelling: application to specialty steels

T. QUATRAVAUX
Laboratoire de Science et Génie des Matériaux et de Métallurgie (UMR 7584), Ecole des Mines, Parc de Saurupt, 54042 Nancy Cedex, France

S. RYBERON, S. HANS
Aubert & Duval Alliages, Etablissement des Ancizes, BP 1, 63770 Les Ancizes Cedex, France

A. JARDY
Laboratoire de Science et Génie des Matériaux et de Métallurgie (UMR 7584), Ecole des Mines, Parc de Saurupt, 54042 Nancy Cedex, France
E-mail: jardy@mines.inpl-nancy.fr

B. LUSSON, P.E. RICHY
Aubert & Duval Alliages, Etablissement des Ancizes, BP 1, 63770 Les Ancizes Cedex, France

D. ABLITZER
Laboratoire de Science et Génie des Matériaux et de Métallurgie (UMR 7584), Ecole des Mines, Parc de Saurupt, 54042 Nancy Cedex, France

A numerical model of the VAR process has been developed at the Ecole des Mines de Nancy over more than 12 years, in close collaboration with industrial partners, to simulate remelting of titanium and zirconium alloys. Nowadays, its applications are extended to specialty steels. Recent studies on the flow modelling highlighted the influence of the turbulence model and the mesh size on the computed evolution of the pool geometry in the upper part of the remelted ingot. Thus, various improvements have been achieved, resulting in a better modelling of the transport phenomena. In particular, a numerical model to simulate the continuous supply of metal in the crucible based on mesh cell splitting and growth has been developed and implemented in the software. The results obtained from the improved version are compared with experimental data from the observation of ingots remelted by Aubert & Duval. The relationship between electromagnetic stirring and the generation of turbulence is investigated from the model results.

1. Introduction

The Vacuum Arc Remelting (VAR) process is currently used to produce high quality specialty steels, nickel-based superalloys, zirconium and titanium alloys. A numerical simulation of the process is being developed within the frame of industrial collaborations between Ecole des Mines and CEZUS, TIMET and Aubert & Duval.

The principle of the VAR process, illustrated in Fig. 1, consists of melting a consumable electrode under a high vacuum, to build up a secondary ingot. During remelting, an electric arc is maintained between the tip of the electrode and the top of the secondary ingot, in order to heat the electrode sufficiently for melting. The liquid metal drops, which fall from the electrode, undergo solidification into the water-cooled crucible. The secondary ingot formed in this way is composed of three distinct zones, namely the liquid pool, fully solidified metal and intermediate mushy zone. The arc can be stabilized and confined with the aid of an axial magnetic field created by an external induction coil. This field is also used to create electromagnetic stirring of the liquid metal flow.

At the Ecole des Mines de Nancy, a computational simulation software, named SOLAR (which stands for SOLidification during Arc Remelting), has been developed over the past decade. It solves the coupled transient heat, momentum and solute transport equations, assuming turbulent liquid metal flow in the melt pool of the remelted ingot [1]. The mathematical model has already been validated by comparison of calculated and experimental liquid pool profiles for Ti and Zr alloy remelted ingots [2–3]. The present paper is devoted to the recent improvements of the model and its use to simulate actual remeltings of ultra-high strength steels and maraging steels. Remelted ingots have been produced

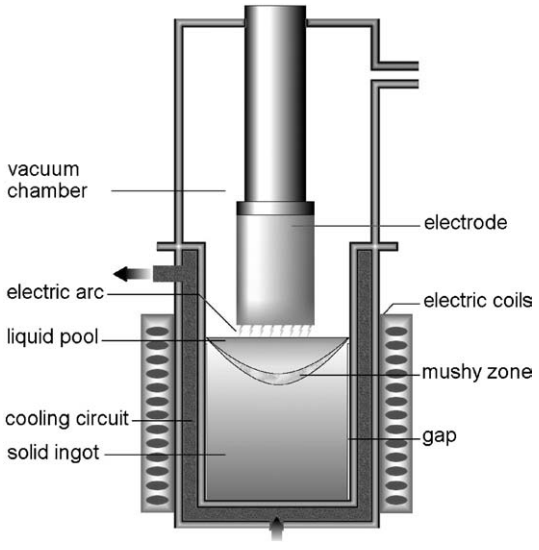

Figure 1 Schematic representation of the VAR process.

by Aubert & Duval to enable comparisons between experimental and calculated results, in particular the pool profiles.

2. Some aspects of the liquid metal flow modelling

Heat transfer in the ingot greatly depends on the recirculation of the flow of liquid metal in the pool, created by buoyancy forces generated by the temperature difference between the heated free surface of the pool and the cooled crucible. Nevertheless, the metal flow is also partly driven by induced electromagnetic forces due to current flow through the ingot, possible magnetic stirring [4] and turbulence generation, which locally modify heat and momentum transfer. Consequences on the pool shape and solidification conditions can be significant, so that our efforts have been focused on the description of the turbulent flow in the liquid pool.

The previous versions of SOLAR software used a simplified k-ε model, which did not take into account buoyancy effects. The model was not well adapted to buoyancy driven flows, so instead the standard $k-\varepsilon$ model [5] has been chosen and is now implemented. This includes full buoyancy effects for the generation and dissipation of turbulence by taking into account an extra source term in the transport equations for k and ε, which depends on the thermal expansion coefficient β and the vertical thermal gradient:

$$G_k \equiv -\beta \frac{\partial T}{\partial z} \tag{1}$$

A program aimed to simulate the steady-state turbulent flow of liquid steel, under thermal and geometrical conditions close to those encountered in a VAR melt pool, has been developed to investigate the influence of mesh scale and refinement on numerical results. As illustrated on Fig. 2, we consider a cylinder, whose radius and height are respectively 0.36 and 0.3 m, in which liquid steel flows because of thermal convection. Furthermore, neither solidification nor electromagnetic forces are taken into account.

At the free surface, on the top of the cylinder, the temperature is fixed (1600°C), as well as at the base

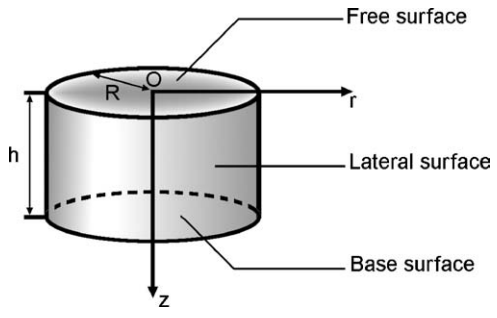

Figure 2 Geometry of the steady-state turbulent flow simulated.

and lateral surfaces (1378°C). Wall functions are used as boundary conditions at these solid/liquid interfaces. At the free surface, the assumed boundary conditions for the momentum transfer equations are the following, where u is velocity:

$$u_{\mathrm{r}}(r, z=0) = 0 \tag{2}$$

$$\frac{\partial u_{\mathrm{r}}}{\partial z}(r, z=0) = 0 \tag{3}$$

$$\frac{\partial k}{\partial z}(r, z=0) = 0 \tag{4}$$

$$\frac{\partial \varepsilon}{\partial z}(r, z=0) = 0 \tag{5}$$

Six meshes, composed of 30×30, 60×60 and 140×140 nodes, with and without a refinement near the top and lateral boundaries, are considered. The refinement was applied to the ten nodes closest to the surfaces, as illustrated on Fig. 3, and consisted of successively reducing the dimensions of adjacent cells by multiplying them by 0.7.

Note that a mesh typically used in SOLAR is made of 30×30 nodes (in the melt pool) without refinement. Maps of normalized temperature (minimum temperature is set to 0 and temperature at the free surface equals 1) and turbulent/molecular viscosity ratio, obtained through simulations using the different meshes, are represented respectively in Figs. 4 and 5.

As can been seen on Fig. 4a2, b2 and c2 all the simulations with refined meshes predict a similar temperature field. However, as illustrated by Fig. 4a1, b1 and c1, notable differences exist between temperature fields obtained with regular meshes. For these simulations, increasing the number of nodes brings the horizontal thermal stratification nearer to the free surface, which produces results close to those obtained by using refined meshes.

Fig. 5 represents computed viscosity ratio maps for the six meshes, where μ is the dynamic viscosity of the liquid metal and μ_{t} is the turbulent viscosity obtained from the k-ε model. These are consistent with the observation made for the temperature field, namely virtually identical fields obtained through simulations using the refined meshes and, for regular meshes, fields closer to the one expected as the number of nodes increases.

It is clear from these figures that, rather than a significant increase in the number of nodes, mesh refinement at the boundaries is essential for a correct simulation of the flow. Although mesh refinement near the crucible was possible in the previous version of SOLAR

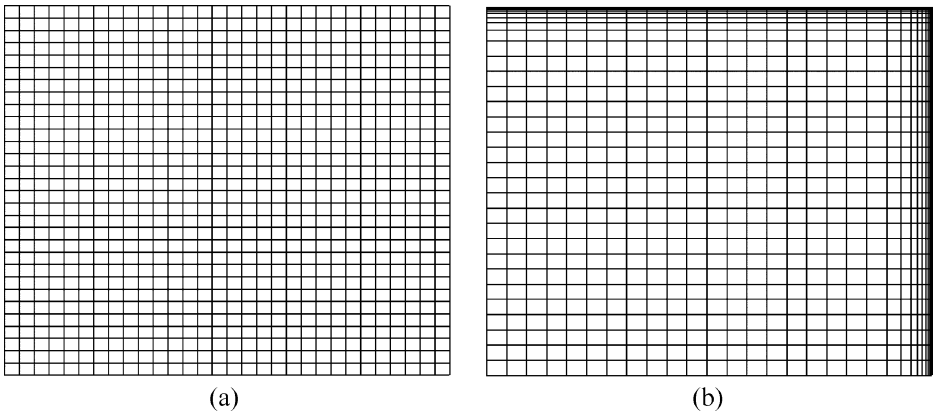

Figure 3 Example of regular (a) and refined (b) meshes used for the simulations.

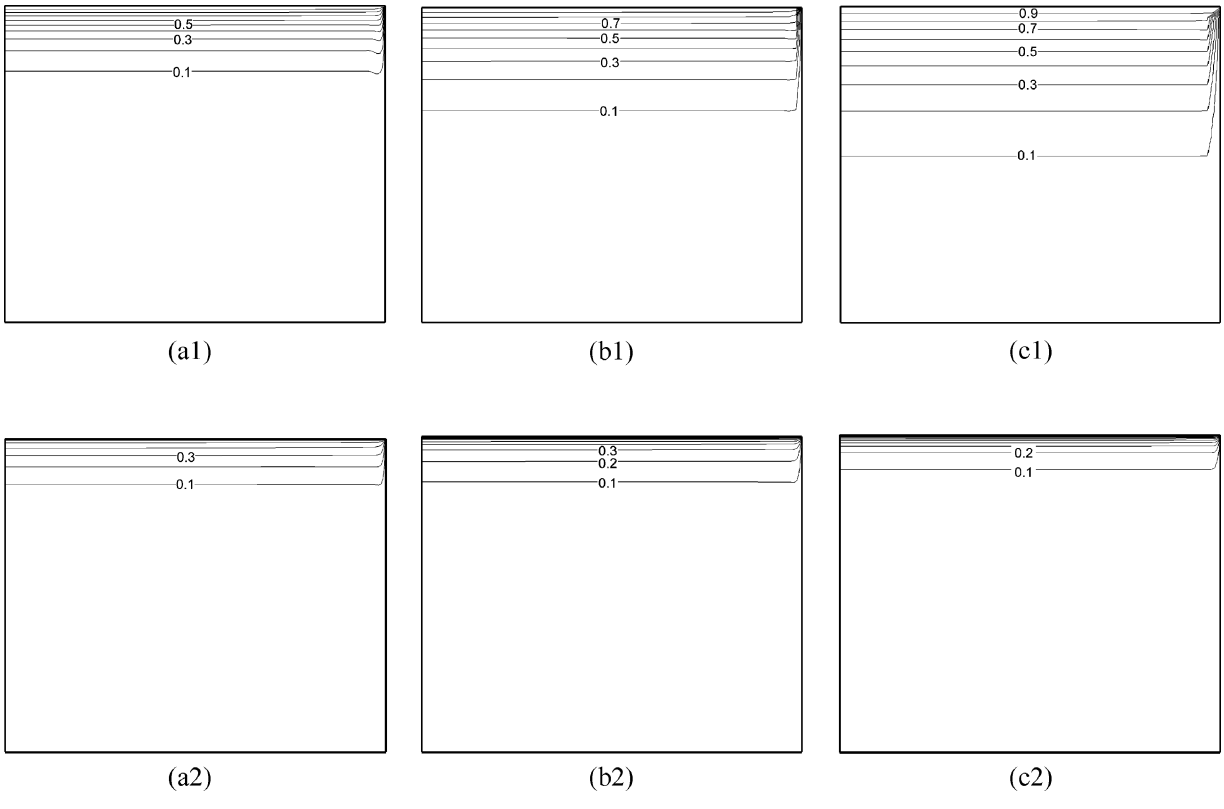

Figure 4 Temperature fields obtained by regular meshes composed of 140 × 140 (a1), 60 × 60 (b1) and 30 × 30 nodes (c1) and by refined meshes composed of 140 × 140 (a2), 60 × 60 (b2) and 30 × 30 nodes (c2).

code, the way of modelling the ingot growth through discontinuous addition of mesh rows precluded any refinement near the free surface. It is our opinion that such a failure could seriously bias the results of the simulations of the metal flow in the pool during remelting.

It is important to notice that for these simulations, where the liquid metal flow is only caused by buoyancy, no significant turbulence was calculated.

3. Improvements of the mathematical model

3.1. Ingot growth modelling

As said previously, the growth of the secondary ingot was previously modelled in SOLAR as a discontinuous process by adding new rows in the mesh, which typically increased from 4 up to 201 rows during the simulation. At the moment of a new row addition, the height of the ingot was supposed to increase instantaneously.

The new model simulates the continuous growth of the ingot during remelting. The technique used consists of splitting the cells of a given line in the mesh, as illustrated on Fig. 6a. Then, the split cells grow to simulate the fall of liquid metal in the crucible, until they reach the size of their neighbours, just before the next split, as shown on Fig. 6b.

This model enables mesh refinement near the free surface to better simulate the flow in the pool, as explained above.

3.2. Modelling of the heat supply at the top of the secondary ingot

As presented elsewhere [6], a new possibility to represent heat supply at the ingot top is to assume a "top hat" distribution of power radiated from the arc to the ingot versus radius. Of course, heat content of liquid

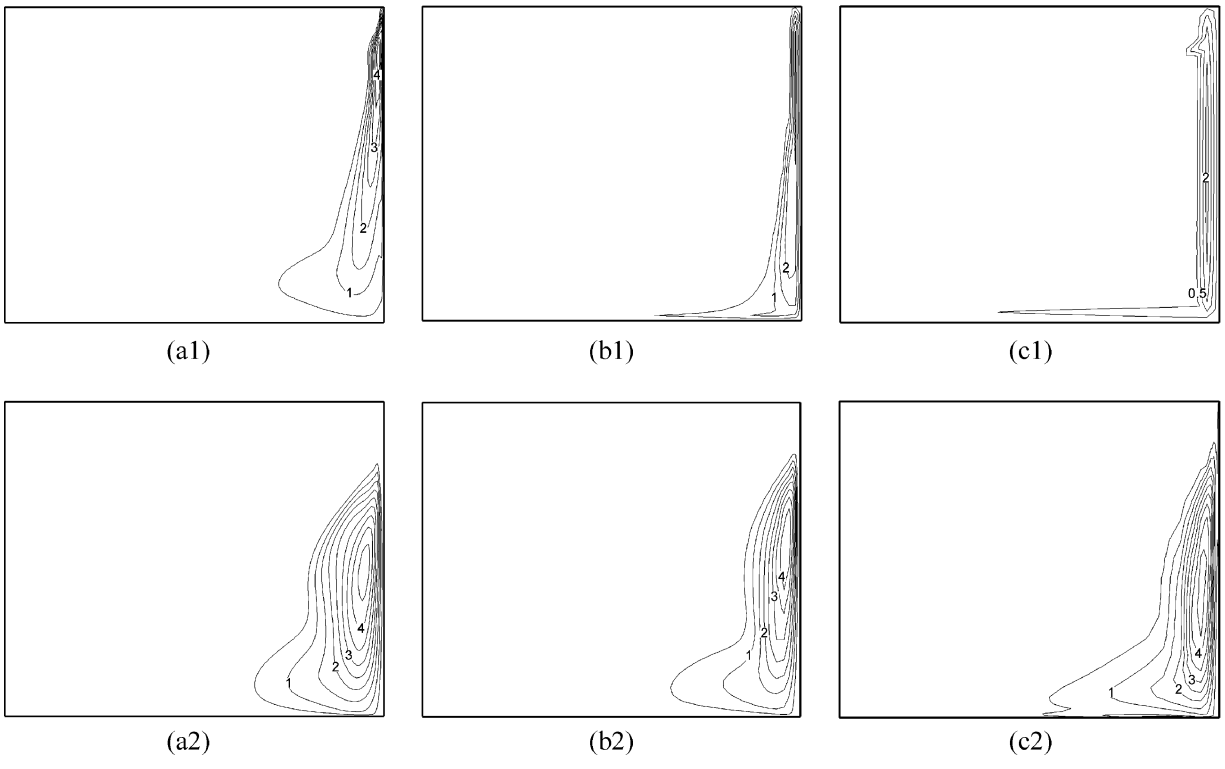

Figure 5 Maps of μ_t/μ ratio obtained by regular meshes composed of 140 × 140 (a1), 60 × 60 (b1) and 30 × 30 nodes (c1) and by refined meshes composed of 140 × 140 (a2), 60 × 60 (b2) and 30 × 30 nodes (c2).

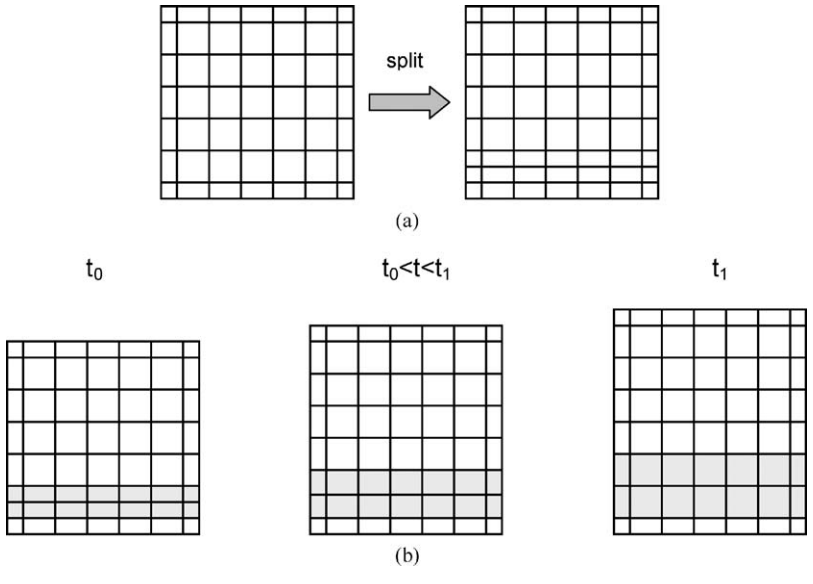

Figure 6 Model of matter supply consisting of cell splitting at time t_0 (a) followed by cell growth and motion from time t_0 to t_1 (b).

metal droplets falling from the electrode is taken into account.

4. Validation of the improved model

Within the frame of an industrial collaboration, the improvements of the mathematical model have to be validated by comparing simulations with experimental results. Validation melts have been realised by Aubert & Duval. In this paper, we will only discuss model validation for the remelting of 4 steel (ultra-high strength steel and maraging steel) ingots. These melts have been stopped before hot-topping in order to mark the liquid pool profiles by microstructural discontinuities, assumed to be formed at 0.5 fraction solid. Then, the ingots were sectioned and etched for structure analysis. For consistency with the experiments, predicted pool profiles are computed as the isovalues of the liquid fraction equal to 0.5. The total heat power on the free surface is supposed to be equal to 80% of the overall electric power [7].

4.1. Ultra-high strength steel

Two 710 mm diameter ingots have been remelted under identical operating conditions, except for electromagnetic stirring. As is shown in Fig. 7, computed pool profiles are superimposed on macrographs. The calculated and experimental profiles are similar in terms of pool depth.

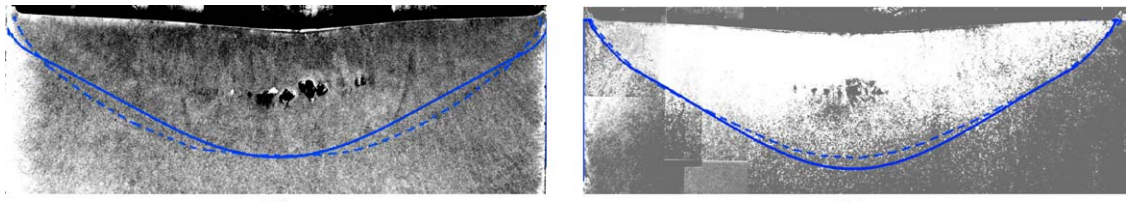

(a) (b)

Figure 7 Comparison of the real and calculated pool profiles (liquid fraction = 0.5)—remelting without electromagnetic stirring (a) and with electromagnetic stirring (b) (dotted lines: experimental—bold: simulation).

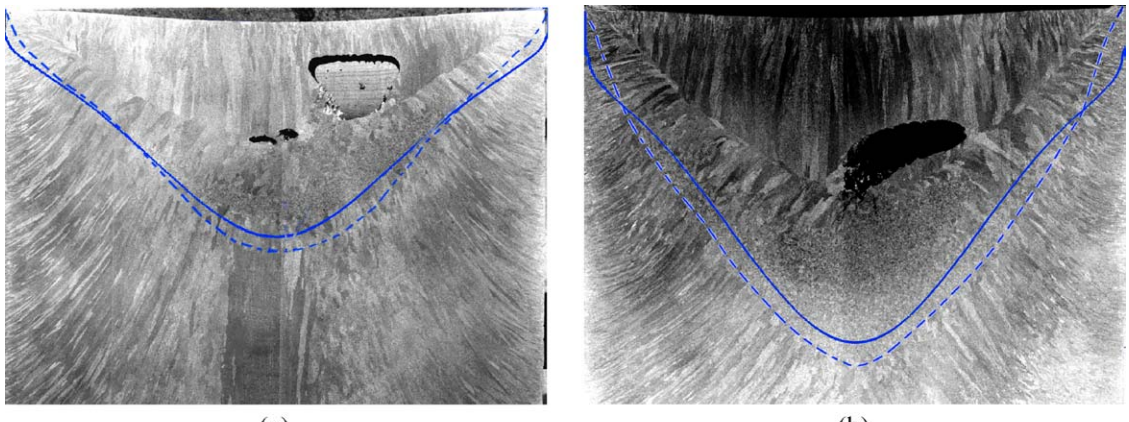

(a) (b)

Figure 8 Comparison of the real and calculated pool profiles (liquid fraction = 0.5)—remelting without electromagnetic stirring, low melt rate (a) and with electromagnetic stirring, high melt rate (b) (dotted lines: experimental—bold: simulation).

Although electromagnetic stirring seems to have no influence on the pool shape, it considerably affects the solidification microstructure by promoting a uniform equiaxed structure instead of the columnar structure obtained with no stirring.

4.2. Maraging steel

Once again, two remeltings of 500 mm diameter ingots have been realised, one without any electromagnetic stirring, with a low melt rate, the second with electromagnetic stirring and a higher melt rate. The experimental pool profiles, at the end of the remelting, are compared to calculated ones in Fig. 8.

It is felt that such comparisons of the calculated pool profiles with the macrographs demonstrate the satisfactory results obtained with the simulations using the improved mathematical model, for a broad range of remelting conditions.

5. Discussion: Electromagnetic stirring and turbulence generation

The model has been used to investigate numerically the influence of various process parameters on the ingot quality. Here, we will study the influence of applying an external magnetic field on the behaviour of the liquid pool hydrodynamics. In the following, "normalized" temperature is equal to 0 for liquidus temperature and 1 for the maximal value.

In order to achieve such a numerical study, remelting of an ultra-high strength steel ingot without any electromagnetic stirring has been simulated. As usual, no significant turbulence is observed in the flow of liquid metal. When the secondary ingot reaches 75% of its final height, a continuous stirring is applied. The predicted evolution of the liquid pool behaviour in the first minute after the application of the stirring is presented below.

In Fig. 9a2 to d2, we can see that the generation of turbulence is located above the mushy zone near the ingot wall. Through comparison with Fig. 9a1 to d1, turbulence intensity can be correlated with an increase in the azimuthal velocity. The figures highlight, in this case, the existence of a critical angular velocity value, equal to approximately 0.04 m s^{-1}, below which no significant turbulence is generated.

Laminarization of the flow near the free surface, which can be observed on Fig. 9a2 and b2, is related to horizontal temperature stratification, which dissipates turbulence in this region. When electromagnetic stirring is applied, the temperature field is more homogeneous near the ingot wall. Turbulence generation then increases thermal transfer between the liquid pool and the crucible, so that cooling is improved. As the thermal stratification decreases, turbulence dissipation is attenuated near the free surface (Fig. 9d2).

The continuous electromagnetic stirring is applied until a new quasi steady-state regime is reached. Fig. 10 highlights differences in the behaviour of the liquid pool under both quasi steady-state regimes, when no stirring is applied and with a constant 1-D (non alternated) electromagnetic stirring (magnetic field of approximately $10^{-3}T$). These regimes are respectively denoted regime 1 and regime 2.

First, it must be noticed that the depth and volume of the pool are larger in regime 2, as is shown on Fig. 10a1 and a2 In both cases, the motion of the metal is made

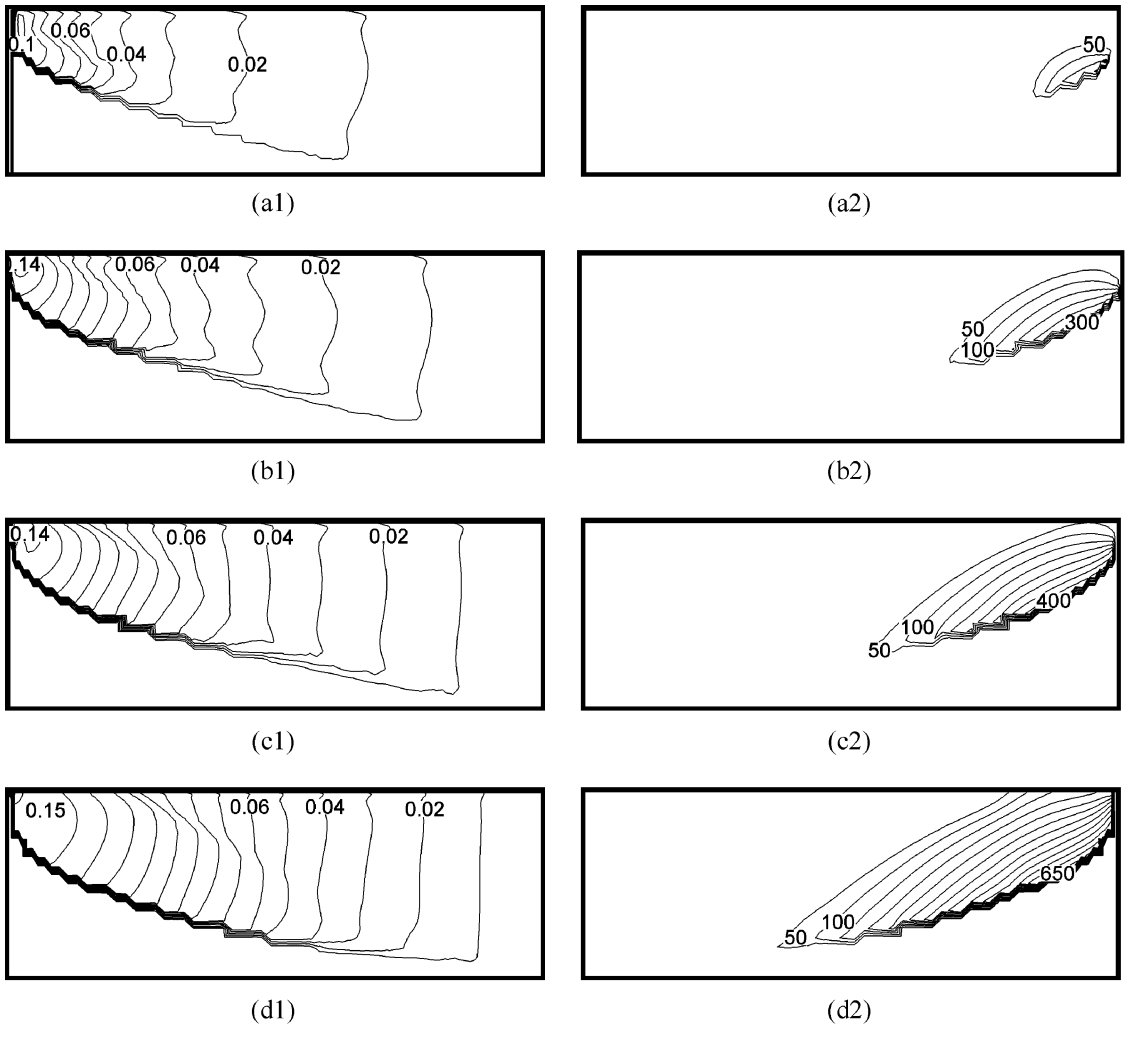

Figure 9 Evolution of angular velocity (m s^{-1}) of the flow (−1) and μ_t/μ viscosity ratio (−2) 15 seconds after the application of the electromagnetic stirring (a), and after 30 s (b), 45 s (c) and 60 s (d).

of only one recirculation loop. Nevertheless, we can see on Fig. 10a2 that, for regime 2, the centre of the vortex is localised at mid-radius near the bottom of the pool, whereas, for regime 1, the centre is close to the lateral wall, near the surface. This difference in the flow pattern is mainly caused by the centrifugal force applied to the liquid pool near the free surface, where stirring is higher [8].

Fig. 10b1 and b2 emphasize the relation between orthoradial stirring and turbulence generation in the flow. Values reached by viscosity ratio, which means the turbulence intensity, are very high in regime 2. This induces a very important additional heat transport, which tends to increase the overall thermal transfer. That explains the homogenisation of the pool temperature in regime 2, compared to regime 1, as is shown on Fig. 10c1 and c2. When stirring is applied, the average pool temperature is lower.

6. Discussion: Effect of the reversal time on the pool behaviour

The model has been used to investigate numerically the influence of various process parameters on the ingot quality. Here, we will study the influence of applying an external magnetic field on liquid pool hydrodynamics. For reasons of confidentiality, we will consider in this chapter the remelting, with a constant melt rate (21 kg/min), of a "fake" alloy, whose thermophysical properties are a mixture of actual properties of Fe-based, Ni-based, Ti-based and Zr-based alloys. Hence, although quantitative results are not significant, the computed qualitative influence of electromagnetic stirring will be well evidenced by the simulations.

Five complete melt simulations have been run. The first one assumes that no external magnetic field is applied. Three simulations consider the application of an external square wave stirring cycle, whose period is either short (40 s), intermediate (2 min) or long (5 min). The fifth simulation considers a constant stirring. In all cases, the field intensity is the same ($10^{-2}T$). Fig. 11 represents the evolution of the computed pool depth for all 5 remeltings. From the figure, it seems obvious that external electromagnetic stirring can have a very big effect on a critical parameter such as the pool depth. However, when stirring is alternated, its period plays a prominent role. When a short period is used, stirring seems to influence only slightly the pool depth. On the other hand, long period alternated stirring is almost equivalent to a constant one, from the same viewpoint.

In order to better understand the physical phenomena underlying such behaviour, it is useful to visualize the

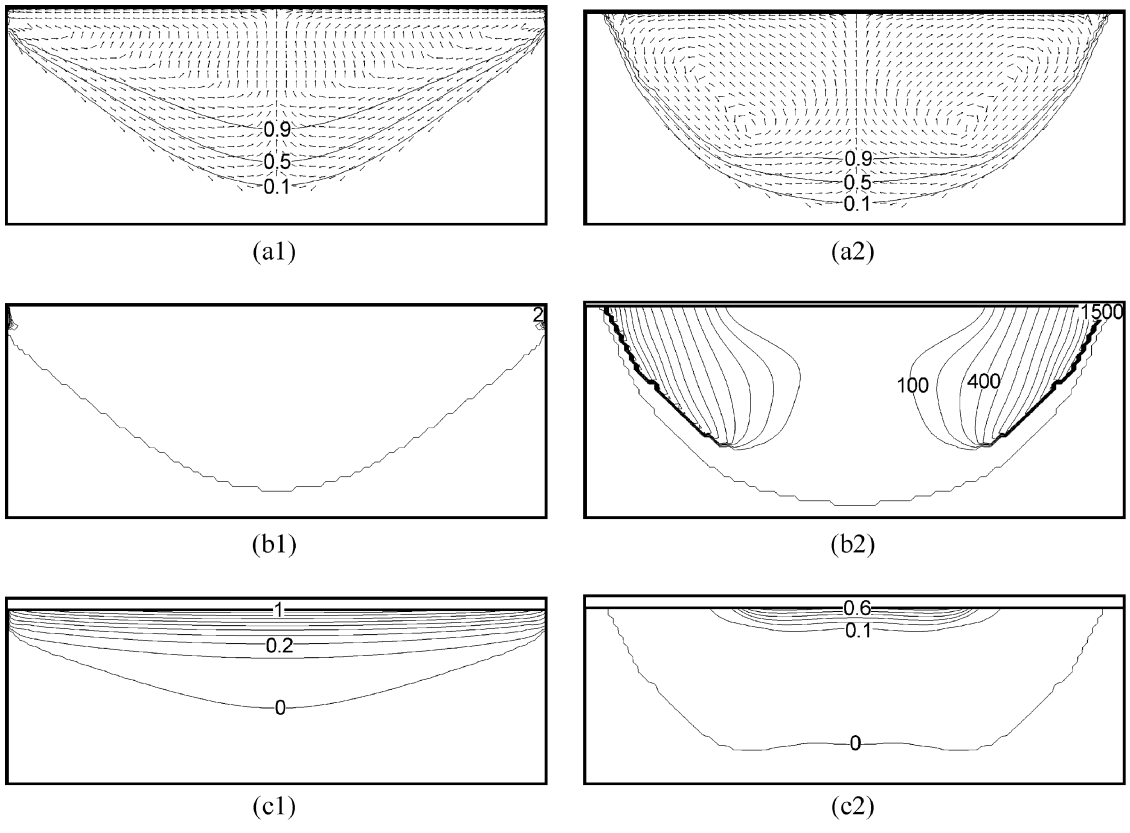

Figure 10 Maps of normalized liquid flow and mushy zone profile (a), μ_t/μ viscosity ratio (b) and normalized temperature (c) in quasi steady-state regime during remelting simulations of ultra–high strength steels without electromagnetic stirring (−1) and with the application of a constant electromagnetic stirring (−2).

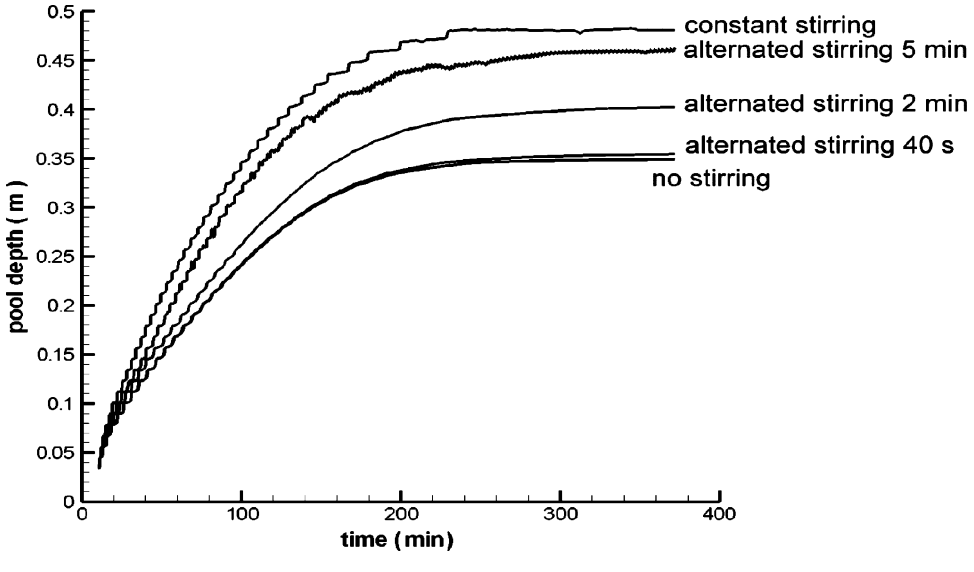

Figure 11 Computed evolution of the liquid pool depth with time for different stirring conditions.

computed flow, particularly the intensity of turbulence. In Fig. 12, the five steady-state pools (mean r-z flow and turbulence intensity) are represented. On the left-hand side, the pool profile is shown (more precisely, the iso-liquid fraction curves 0.1 and 0.9), along with the flow pattern in the r-z plane. The figure clearly shows that varying the stirring reversal time directly affects the flow and in particular the turbulence level.

When no stirring is applied, the fluid flow, driven by buoyancy and induced electromagnetic forces, is very weak and laminar. Applying a short period electromagnetic stirring does not change that behaviour. Such a finding is consistent with the experimental evidence reported in Fig. 7. On the other hand, constant stirring results in a strong circular motion. Thus, centrifugal forces predominate and the r-z flow is also stronger. Turbulence intensity becomes very high, heat transfer is greatly enhanced and the pool deepens. Long period alternated stirring has the same effect, because turbulence can fully develop during each half of the cycle.

These findings, together with results reported on Fig. 9, explain easily the influence of the stirring period on the hydrodynamic behaviour and the melt pool depth. When stirring is rapidly reversed, the

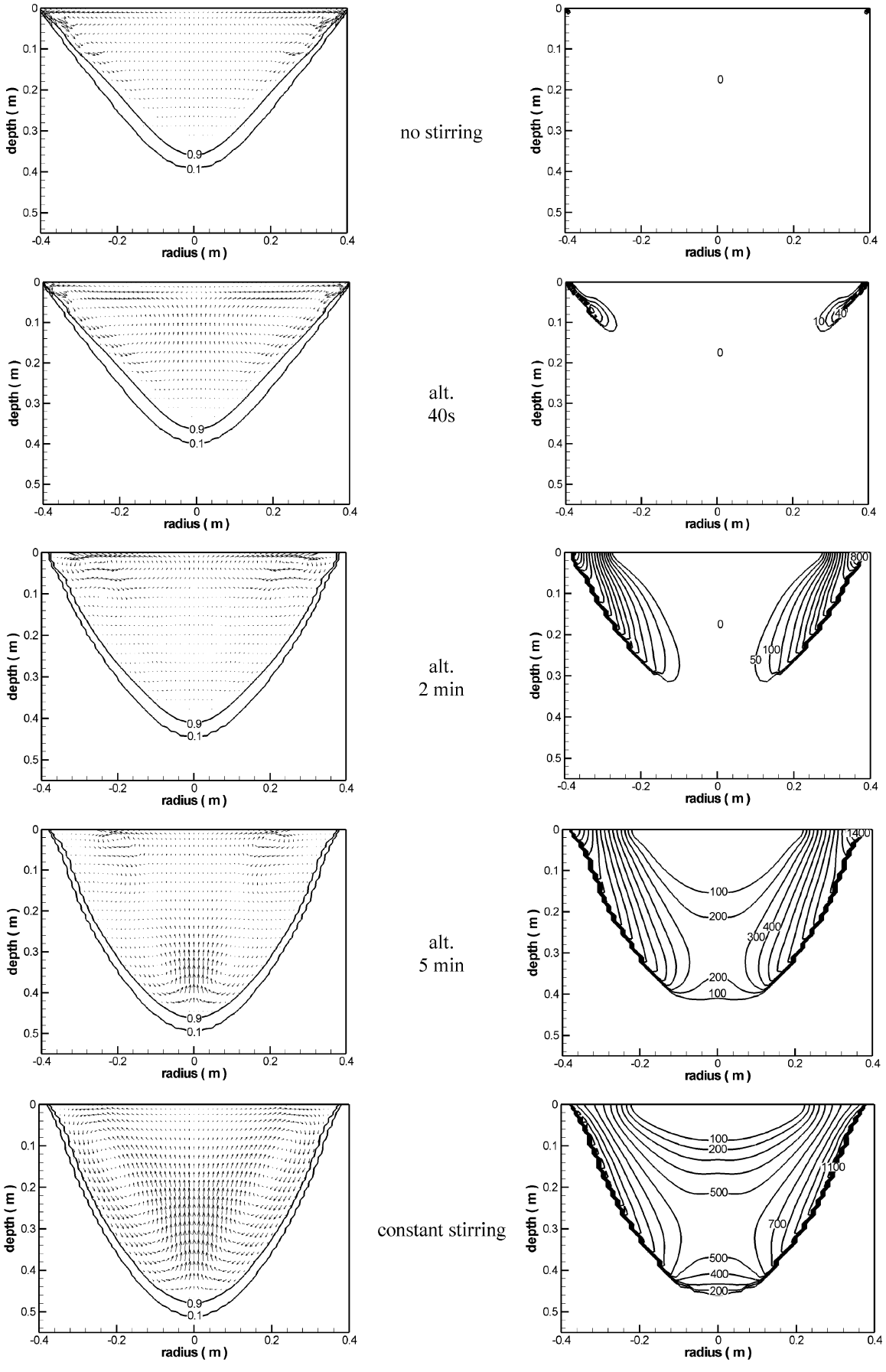

Figure 12 Steady-state hydrodynamic behaviour of the melt pool for different stirring conditions—(r, z) motion of the metal (left) and μ_t/μ viscosity ratio (right).

angular velocity remains low and turbulence is not generated.

7. Conclusion

The mathematical model which constitutes the SOLAR software has been recently improved in several ways to better simulate fluid flow and heat transfer in the liquid metal pool. A new model for the mesh growth has been developed to represent accurately the continuous supply of metal in the crucible. Furthermore, the standard $k-\varepsilon$ model has been implemented to simulate turbulent flow.

The comparison between experimental and numerical results validates the use of the new mathematical model, which enables mesh refinement near the free surface, to simulate the remelting of various steel ingots.

An investigation into the sensitivity of the results of simulation of steady-state turbulent flow highlights the influence of mesh refinement near the lateral wall and the free surface. For melts with no stirring and with shallow pools such as those encountered for special steels and superalloys with helium cooling (by comparison with pools obtained for reactive metals melts such as Ti or Zr with no helium cooling), an important result is that the thermal stratification reduces turbulence generation and that the flow is almost laminar. However, changes in melt pool hydrodynamics can occur within a short time interval (<60 s) after application of electromagnetic stirring and promote turbulence generation especially near the lateral wall. Stirring, either continuous or alternated with a sufficiently large reversal time, modifies consequently the pool shape, flow recirculation and thermal field. These differences are the consequence of turbulence generation.

This model is currently used by Aubert & Duval as a tool to optimise the melting conditions of various specialty steel ingots.

References

1. S. HANS, Modélisation des transferts couples de chaleur, de solute et de quantité de movement lors de la refusion à l'arc sous vide (VAR)—Application aux alliages de titane, Ph.D. thesis, INPL (1995).
2. S. HANS, A. JARDY and D. ABLITZER, in Proceedings of the Int. Symp. on Liquid Metal Processing and Casting, edited by A. Mitchell and J. Fernihough, Santa Fe, New Mexico, 1994, p. 143.
3. A. JARDY, A. F. WILSON, D. LASALMONIE and D. ABLITZER, in Proceedings of the Int. Symp. on Liquid Metal Processing and Casting, edited by A. Mitchell and J. Van Den Avyle, Santa Fe, New Mexico, 2001, p. 200.
4. P. A. DAVIDSON, X. HE and A. J. LOWE, *Mater. Sci. Techn.* **16** (2000) 699.
5. S. B. POPE, "Turbulent Flows" (Cambridge University Press, Cambridge, UK, 2000) p. 373.
6. P. CHAPELLE, H. EL MIR, J. P. BELLOT, A. JARDY, D. ABLITZER and D. LASALMONIE, *J. Mater. Sci.*, this issue.
7. A. JARDY, L. FALK and D. ABLITZER, *Ironmak. Steelmak.* **19**(3) (1992) 226.
8. D. ABLITZER, A. JARDY and J. P. BELLOT, in Proceedings of the 4th Symp. on Adv. Tech. and Proc. for Metals and Alloys, edited by ALD Vacuum Technologies AG, Frankfurt, Germany, 1999, p. 103.

Received 17 March
and accepted 10 June 2004